

Model of light collimation by photonic crystal surface modes

Wojciech Śmigaj*

Surface Physics Division, Faculty of Physics, Adam Mickiewicz University, Umultowska 85, 61-614 Poznań, Poland

(Received 20 December 2006; revised manuscript received 22 March 2007; published 21 May 2007)

We propose a quantitative model explaining the mechanism of light collimation by leaky surface modes that propagate on a corrugated surface around the output of a photonic crystal waveguide. The dispersion relation of these modes is determined for a number of surface terminations. Analytical results obtained on the basis of the model are compared to those of rigorous numerical simulations. Maximum collimation is shown to occur at frequency values corresponding to excitation of surface modes whose wave number retains a *nonzero* real part.

DOI: 10.1103/PhysRevB.75.205430

PACS number(s): 42.70.Qs, 42.79.Ag, 78.68.+m

I. INTRODUCTION

One of the problems hindering wider commercial application of photonic crystals (PCs) is the difficulty in coupling PC waveguides to conventional dielectric waveguides or optical fibers. A possible solution consists in tapering the waveguide so as to achieve better coupling with the fiber; this has been the subject of a number of publications, e.g., Refs. 1 and 2. Recently, Moreno *et al.*³ and Kramper *et al.*⁴ independently suggested that collimation of the light emitted by a waveguide (*beaming*) could also occur due to excitation of surface modes in the proximity of the waveguide exit. Based on the earlier discovery of a similar effect in metallic structures supporting surface plasmons,⁵ the idea has been expanded in several articles following the original papers.^{6–11}

Moreno *et al.* propose a simple qualitative theory to explain the novel effect.³ The radiation reaching the waveguide outlet can couple to surface modes; if the surface around the outlet is *corrugated* (i.e., modulated with period different from that of the underlying crystal), its eigenstates become “leaky,” since energy is emitted as the radiation scatters at the perturbed surface cells. Under appropriate conditions, the scattered waves interfere constructively along the surface normal, thus producing a collimated beam. According to Ref. 3, this constructive interference takes place for surface modes of wave vector $k_x=0$ (shifted to the first Brillouin zone of the surface), with the phase difference between two successive scatterers equal to an integer multiple of 2π .

The purpose of this work is to formulate a quantitative model of the beaming effect in PCs, taking explicitly into account the imaginary component of the leaky-mode wave vector. The model predictions are tested against results of numerical simulations. We also show that, for practically realizable PCs, maximum beaming occurs for surface modes with $\text{Re } k_x \neq 0$.

II. MODEL

The system to be considered is depicted in Fig. 1. Excited by a source at the waveguide input (left), a guided mode propagates towards the crystal surface (right). On reaching the output, the radiation is partially reflected, partially emitted directly into free space, and the remainder excites leaky modes propagating upward and downward along the surface

corrugated with period Λ . Either side of the waveguide comprises N surface unit cells. Our aim is to calculate the radiation intensity $\Phi(\theta)$ defined as

$$\Phi(\theta) \equiv \lim_{r \rightarrow \infty} r S_r(r, \theta), \quad (1)$$

where $S_r(r, \theta)$ denotes the radial component of the time-averaged Poynting vector at the point specified by the polar coordinates (r, θ) .

Without losing generality, we restrict our attention to E polarization (with the electric field parallel to the cylinder axes). Since all sources of the electromagnetic field are lo-

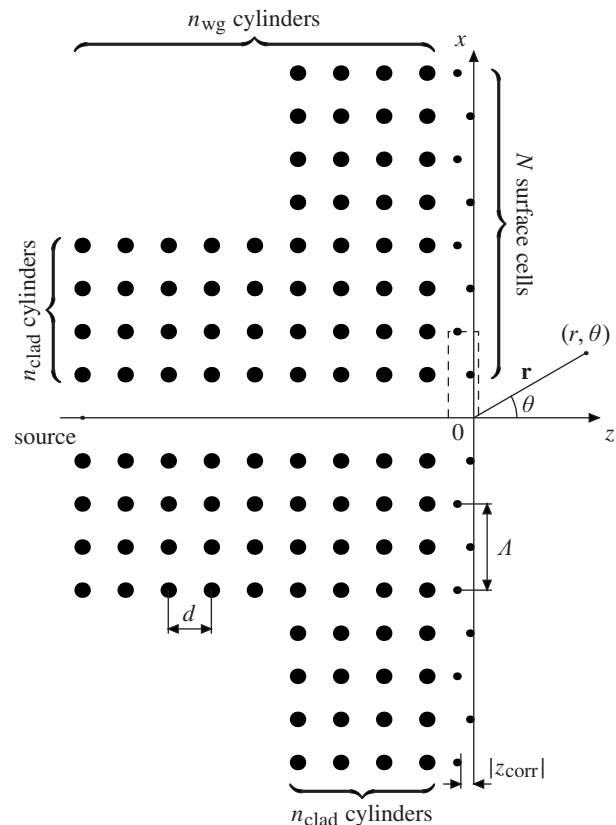


FIG. 1. A waveguide embedded in a PC with corrugated surface.

cated in the $z < 0$ half space, the crystal can be regarded as an aperture antenna, with radiation pattern proportional to the Fourier transform of the electric-field distribution at the $z = 0$ axis,¹²

$$\mathbf{E}(r, \theta) \simeq \hat{\mathbf{y}} e^{i(k_0 r - \pi/4)} \frac{k_0}{\sqrt{k_0 r}} f(k_0 \sin \theta) \cos \theta, \quad (2a)$$

where

$$f(k_0 \sin \theta) \equiv \frac{1}{\sqrt{2\pi}} \int_{-\infty}^{\infty} E_y(x, 0) e^{-ik_0 x \sin \theta} dx, \quad (2b)$$

$k_0 \equiv \omega/c$ denotes the free-space wave number and r is assumed to be large compared to the system dimensions. Since the crystal is symmetric with respect to the z axis, $E_y(x, 0) = E_y(-x, 0)$ and

$$f(k_0 \sin \theta) = f^+(k_0 \sin \theta) + f^+(-k_0 \sin \theta), \quad (3)$$

where $f^+(k_0 \sin \theta)$ is defined as

$$f^+(k_0 \sin \theta) \equiv \frac{1}{\sqrt{2\pi}} \int_0^{\infty} E_y(x, 0) e^{-ik_0 x \sin \theta} dx. \quad (4)$$

The field $E_y(x, 0)$ consists basically of three major components: the beam stemming directly from the waveguide outlet [$E_y^{\text{wg}}(x, 0)$], the leaky mode propagating along the corrugated surface [$E_y^{\text{surf}}(x, 0)$], and the residual radiation extending past the crystal boundaries [$E_y^{\text{res}}(x, 0)$]. In this section, we focus on the surface-mode contribution, assuming that $E_y(x, 0) = E_y^{\text{surf}}(x, 0)$; the effect of the other components is discussed in Sec. IV.

Neglecting the fringe effects at the surface boundaries, we can apply the Bloch theorem to the field related to the leaky mode. This yields

$$E_y^{\text{surf}}(x, 0) = \begin{cases} u \left(|x| - \frac{d}{2} \right) e^{ik_x (|x| - d/2)} & \text{if } 0 < |x| - \frac{d}{2} < N\Lambda \\ 0 & \text{otherwise.} \end{cases} \quad (5)$$

Function $u(x)$ is Λ periodic and $k_x \equiv k'_x + ik''_x$ ($k''_x > 0$) denotes the leaky-mode wave number. We assume that the waveguide output has effective width d , which is the lattice constant of the underlying PC, and do not consider this area to belong to the crystal surface. With Eq. (5) substituted into Eq. (4), we get through integration,

$$\begin{aligned} f^+(k_0 \sin \theta) &= \left[\sum_{n=0}^{N-1} e^{i(k_x - k_0 \sin \theta) n \Lambda} \right] e^{-i(k_0 \sin \theta) d/2} F(k_0 \sin \theta) \\ &= \frac{1 - e^{i(k_x - k_0 \sin \theta) N \Lambda}}{1 - e^{i(k_x - k_0 \sin \theta) \Lambda}} e^{-i(k_0 \sin \theta) d/2} F(k_0 \sin \theta), \end{aligned} \quad (6)$$

where the *structure factor* $F(k_0 \sin \theta)$ is defined as

$$F(k_0 \sin \theta) \equiv \frac{1}{\sqrt{2\pi}} \int_0^{\Lambda} u(x) e^{i(k_x - k_0 \sin \theta) x} dx. \quad (7)$$

Being a periodic function, $u(x)$ can be Fourier expanded,

$$u(x) = \sum_{n=-\infty}^{\infty} u_n e^{2\pi i n x / \Lambda}, \quad (8)$$

resulting in the following form of the formula for $F(k_0 \sin \theta)$,

$$\begin{aligned} F(k_0 \sin \theta) &= \frac{1}{\sqrt{2\pi}} \sum_n u_n \int_0^{\Lambda} e^{i(k_x + 2\pi n / \Lambda - k_0 \sin \theta) x} dx \\ &= \frac{1}{\sqrt{2\pi}} \sum_n u_n \frac{e^{i(k_x - k_0 \sin \theta) \Lambda} - 1}{i(k_x + 2\pi n / \Lambda - k_0 \sin \theta)}. \end{aligned} \quad (9)$$

In the first approximation, which is often used in analytical treatment of leaky-wave antennas,¹³ only the term with denominator of the smallest magnitude (the zeroth term in the case of near-zero k_x) needs to be kept in the above sum. Substitution of this approximate structure factor into Eq. (9) leads to

$$f^+(k_0 \sin \theta) = \frac{i u_0}{\sqrt{2\pi}} \frac{1 - e^{i(k_x - k_0 \sin \theta) N \Lambda}}{k_x - k_0 \sin \theta} e^{-i(k_0 \sin \theta) d/2}. \quad (10)$$

From the Maxwell equations, it can be shown that in vacuum

$$S_r(r, \theta) = \frac{1}{2Z_0} |E(r, \theta)|^2 \quad \text{with } Z_0 \equiv \sqrt{\frac{\mu_0}{\epsilon_0}}. \quad (11)$$

Therefore, using Eqs. (2a), (3), (10), and (11), and definition (1), we arrive at

$$\begin{aligned} \Phi(\theta) &= \frac{k_0}{4\pi Z_0} |u_0|^2 \cos^2 \theta \left| \frac{1 - e^{i(k_x - k_0 \sin \theta) N \Lambda}}{k_x - k_0 \sin \theta} \right. \\ &\quad \left. + \frac{1 - e^{i(k_x + k_0 \sin \theta) N \Lambda}}{k_x + k_0 \sin \theta} \right|^2. \end{aligned} \quad (12)$$

The unknown coefficient u_0 can be determined from the principle of energy conservation. Consider a semi-infinite section of the crystal surface along which the leaky mode in question propagates. By a procedure analogous to that followed above, we obtain the radiation intensity generated by the leaky wave in this configuration,

$$\Phi(\theta) = \frac{k_0}{4\pi Z_0} |u_0|^2 \frac{\cos^2 \theta}{|k_x - k_0 \sin \theta|^2}. \quad (13)$$

Integrated over the interval $[-\frac{\pi}{2}, \frac{\pi}{2}]$, this yields the total power radiated into free space, which must be equal to the power P_0 exciting the leaky mode. Therefore,

$$P_0 = \frac{k_0}{4\pi Z_0} |u_0|^2 \int_{-\pi/2}^{\pi/2} \frac{\cos^2 \theta}{|k_x - k_0 \sin \theta|^2} d\theta. \quad (14)$$

The integral in the above equation can be evaluated analytically. Thus,

$$|u_0|^2 = \frac{4\pi Z_0 k_0 P_0}{J(k_x/k_0)}, \quad (15)$$

where

$$\begin{aligned}
 J(\kappa) \equiv & -\pi - \frac{1}{i \operatorname{Im} \kappa} \left\{ \sqrt{\kappa^2 - 1} \left[\arctan \frac{1 - \kappa}{\sqrt{\kappa^2 - 1}} \right. \right. \\
 & - \arctan \frac{1 + \kappa}{\sqrt{\kappa^2 - 1}} \left. \right] - \sqrt{(\kappa^*)^2 - 1} \left[\arctan \frac{1 - \kappa^*}{\sqrt{(\kappa^*)^2 - 1}} \right. \\
 & \left. \left. - \arctan \frac{1 + \kappa^*}{\sqrt{(\kappa^*)^2 - 1}} \right] \right\}. \quad (16)
 \end{aligned}$$

By substituting Eq. (15) into Eq. (12), we obtain the final formula for the radiation intensity in the system shown in Fig. 1, normalized to the accepted power P_0 and expressed solely in terms of the leaky surface-mode parameters,

$$\frac{\Phi(\theta)}{P_0} = \frac{k_0^2 \cos^2 \theta}{J(k_x/k_0)} \left| \frac{1 - e^{i(k_x - k_0 \sin \theta)N\Lambda}}{k_x - k_0 \sin \theta} + \frac{1 - e^{i(k_x + k_0 \sin \theta)N\Lambda}}{k_x + k_0 \sin \theta} \right|^2. \quad (17)$$

III. NUMERICAL DETERMINATION OF SURFACE MODES

To apply the above-discussed model to a specific photonic surface, e.g., for the determination of the frequency most conducive to beaming, it is necessary to calculate the dispersion relation of the modes supported by the surface. In this section, we shall briefly outline the method we employed for this purpose.

In our approach, we consider a semi-infinite PC with possible surface reconstruction. The whole system is divided into three parts: the homogeneous region, the surface, and the underlying semi-infinite, but otherwise ideal, photonic crystal. The electromagnetic field in the homogeneous material is represented as a Rayleigh expansion, i.e., a linear combination of discrete plane waves, whereas in the semi-infinite crystal the field is expanded into the eigenmodes of the corresponding infinite structure (a procedure suggested by Istrate *et al.*¹⁴). Since we are searching for states leaking energy away from the surface, in both regions we only consider waves that propagate or decay in this direction; the precise rules of choosing these waves are specified in the Appendix. The complex band structure necessary to find the field representation in the PC is calculated by the differential method (see Ref. 15 for details).

The fields in the homogeneous region and in the PC are linked by the scattering matrix¹⁵ of the surface layer, which provides the necessary boundary conditions. This leads to a homogeneous system of linear equations, which must have a nontrivial solution for surface states to exist. The search for surface modes is thus reduced to a search for roots of the determinant of a matrix dependent on k'_x , k''_x , and ω .

IV. RESULTS

A. Surface-mode dispersion

In the following, we shall focus on crystals of the type shown in Fig. 1, considering a truncated square lattice of dielectric cylinders of permittivity $\epsilon=11.56$ embedded in vacuum, with bulk cylinder radius $0.18d$, surface cylinder

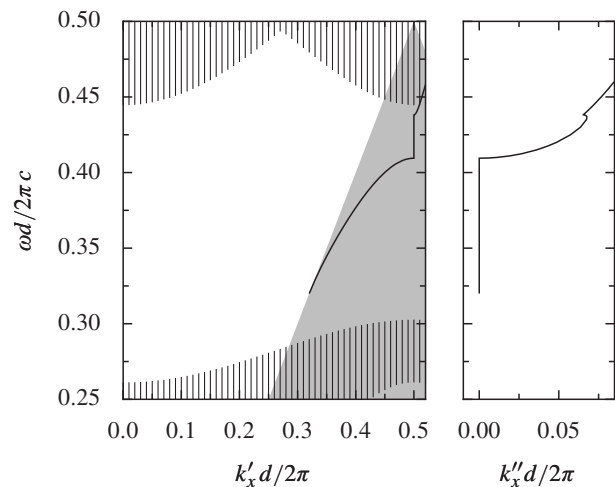


FIG. 2. Crystal A surface-mode dispersion curve. The hatched areas represent bulk bands, and the gray triangle denotes the bounded-wave region, in which all spatial harmonics are evanescent in vacuum for $k''_x=0$.

radius $0.09d$, surface corrugation period $\Lambda=2d$, and three values of corrugation depth z_{corr} : $0, -0.1d$, and $-0.3d$ (the minus sign indicates that the perturbed cylinders are shifted toward the crystal). For future reference, we denote these three crystals with letters A, B, and C, respectively. Figure 2 presents the dispersion curve of surface modes supported by crystal A (in the extended Brillouin-zone scheme), while in Fig. 3 the dispersion curves corresponding to crystals B and C are plotted in the vicinity of the center of their first Brillouin zone. All these dispersion relations have been determined by the method described in the previous section. Only the modes with $k''_x \geq 0$ are shown.

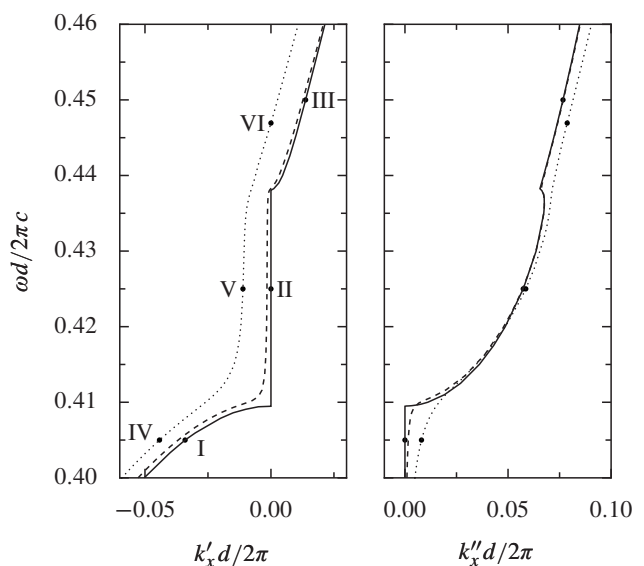


FIG. 3. Crystals B and C surface-mode dispersion curves (dashed and dotted lines, respectively) in the vicinity of the center of the first Brillouin zone. The solid line represents a segment of crystal A dispersion curve from Fig. 2, shifted by $\Delta k_x = -\pi/d$ and shown for comparison.

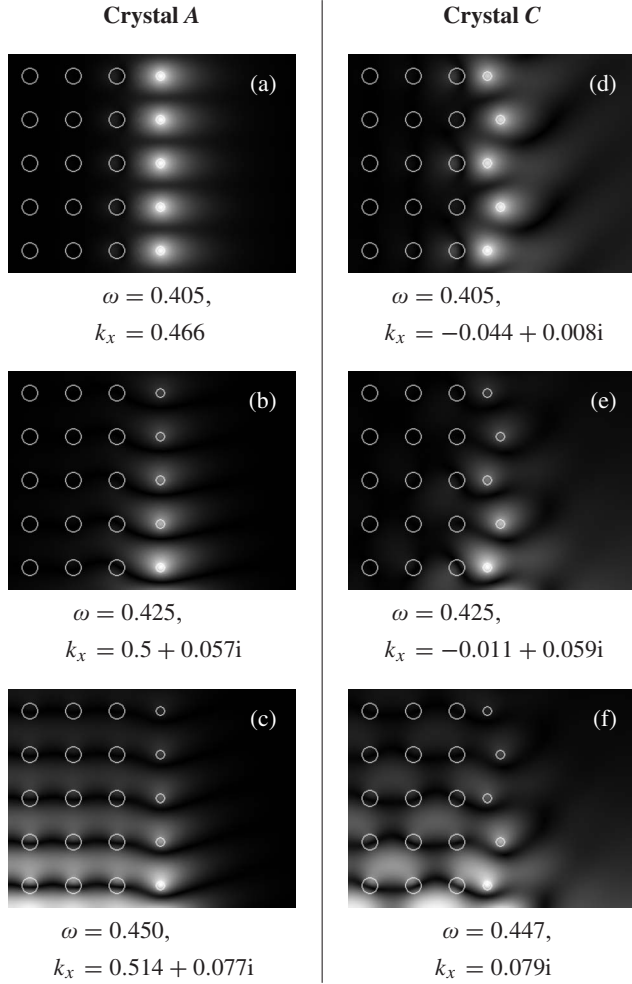


FIG. 4. [(a)–(f)] Maps of the electric-field magnitude for surface modes labeled I–VI in Fig. 3. The frequency and wave number values are expressed in units of $2\pi c/d$ and $2\pi/d$, respectively.

In the frequency range $\omega < 0.409 \times 2\pi c/d$, crystal *A* supports proper (nonleaky, i.e., with $k_x''=0$) surface waves, since this fragment of the dispersion curve lies in the bounded-wave region (shaded in Fig. 2), in which all spatial harmonics are evanescent in vacuum. Figure 4(a) shows the field map of a sample mode from this part of the dispersion curve. The range $0.409 < \omega d/2\pi c < 0.438$ corresponds to a stop band, where the surface-mode wave number takes values of $\pi/d + ik_x''$; see Fig. 4(b) for the field map of a typical stop-band state. Characteristic for periodic structures, the occurrence of a stop band at the Brillouin-zone boundary has been observed in surface-mode dispersion relations of periodic dielectric waveguides embedded in homogeneous media.^{16,17} In contrast, the shape of the dispersion curve at $k_x' > \pi/d$ stems directly from the presence of the underlying PC, i.e., from the periodicity of the “substrate.” Although the dispersion curve remains within the bounded-wave region, the surface-mode wave number retains a large imaginary part, since the wave leaks energy *into the crystal*, as can be observed in Fig. 4(c), showing the field magnitude of the mode labeled III in Fig. 3. This field structure is analogous to that of leaky modes propagating in periodic waveguides adjacent

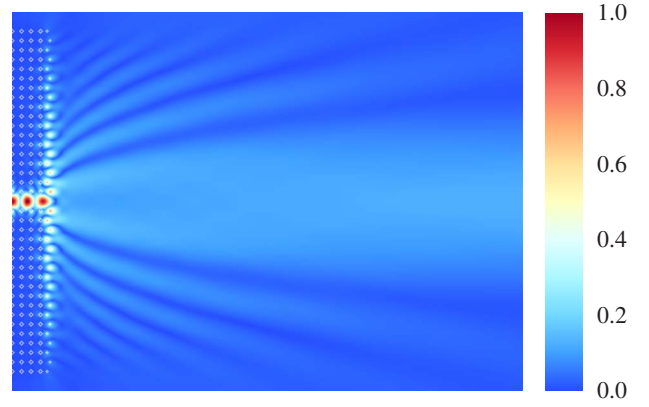


FIG. 5. (Color online) Electric-field magnitude for crystal *C* with $N=9$ corrugated surface cells at frequency $\omega = 0.410 \times 2\pi c/d$.

to homogeneous media: the wave amplitude in the PC grows as $z \rightarrow -\infty$. As observed in early studies of leaky waves,¹⁸ this behavior is not unphysical, since in real systems the field extent is limited by the location of the source exciting the leaky wave.

Let us proceed to the case of nonzero corrugation (crystals *B* and *C*). Doubling the surface period results in the first Brillouin zone folding away to the range $[-\pi/2d, \pi/2d]$; consequently, at frequency values above $0.25 \times 2\pi c/d$, at least one spatial harmonic is radiative and the originally bound surface states become leaky. As shown in Fig. 3, the surface-mode dispersion curve smooths out, shifting toward negative k_x' and larger positive k_x'' , as the corrugation depth increases. Interestingly, at frequency values above $0.438 \times 2\pi c/d$, the substrate PC supports bulk states characterized by essentially imaginary k_x ($k_x \approx ik_x'' \approx 0.66i \times 2\pi/d$) and *purely real* k_z . In consequence, in all three crystals considered here, the leaky modes from the immediate vicinity of the $k_x'=0$ line are propagative in the $-z$ direction. Therefore, this line serves as a boundary between leaky modes exponentially decaying ($k_x' < 0$) and growing ($k_x' > 0$) inside the substrate. Figures 4(d)–4(f) show maps of the field corresponding to points IV–VI on the dispersion curve of crystal *C*.

B. Light collimation: Frequency dependence

Let us now proceed to the analysis of beaming itself. Figure 5 presents the electric-field magnitude calculated by the multiple-scattering (MS) method (see Ref. 19 for details), with geometry parameters and frequency value conducive to directional emission. In Fig. 6, the frequency dependence of the radiation intensity $\Phi_{\text{sim}}(\theta=0)$ calculated by the MS method is compared to that obtained on the basis of our model, for crystals *B* and *C* with $N=9$ and $N=15$ corrugations. In these MS simulations, we consider the system depicted in Fig. 1, with the waveguide $n_{\text{wg}}=12$ cylinders long and cladding $n_{\text{clad}}=5$ cylinders wide; a waveguide mode is excited by a point source near the inlet. The results depicted in Fig. 6 clearly show that our model reproduces the basic feature of the effect in question, i.e., the existence of a distinct transmission maximum at a well-defined frequency

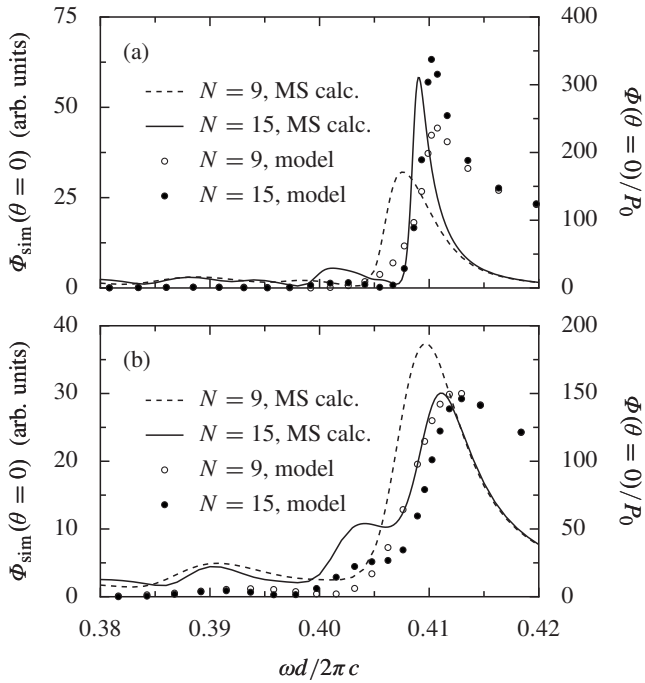


FIG. 6. Frequency dependence of the collimated beam intensity for crystals B (a) and C (b). The left and right y axes refer to the results of MS calculations (lines) and the model predictions (circles), respectively.

value. The relative height of the $\Phi_{\text{sim}}(\theta=0)$ curve peaks for different crystals is rendered reasonably well too. There are some visible differences between the model predictions and the simulation results, though. Most notably, the absolute maxima in the theoretical curves are shifted by approximately $0.002 \times 2\pi c/d$ to the right with respect to those found numerically. Furthermore, at frequency values smaller (larger) than those corresponding to the main peaks, the model generally predicts radiation intensity values several times smaller (larger) than those calculated numerically. Possible causes of these discrepancies are analyzed in the following subsection by scrutinizing the angular dependence of the radiation intensity.

C. Light collimation: Angular dependence

Figure 7(a) shows the angular dependence of the radiation intensity $\Phi_{\text{sim}}(\theta)$ calculated by the MS method for crystal C with $N=9$ corrugations at frequency $\omega=0.400 \times 2\pi c/d$. To help evaluate the relative importance of the three regions mentioned in Sec. II—the waveguide outlet, the corrugated surface, and the crystal exterior—we have also plotted separately the contributions of sections $|x| < d/2$, $d/2 < |x| < N\Lambda + d/2$, and $|x| > N\Lambda + d/2$, calculated by aperture formula (2) with the values of $E_y(x,0)$ obtained by the MS method. The radiation intensity produced by each of these regions will be labeled $\Phi_{\text{sim}}^{\text{wg}}$, $\Phi_{\text{sim}}^{\text{surf}}$, and $\Phi_{\text{sim}}^{\text{res}}$, respectively.

The graph shows that while surface modes play the most important part and are responsible for the formation of the major lobes, the radiation coming directly from the waveguide outlet has an impact as well. In particular, it makes the

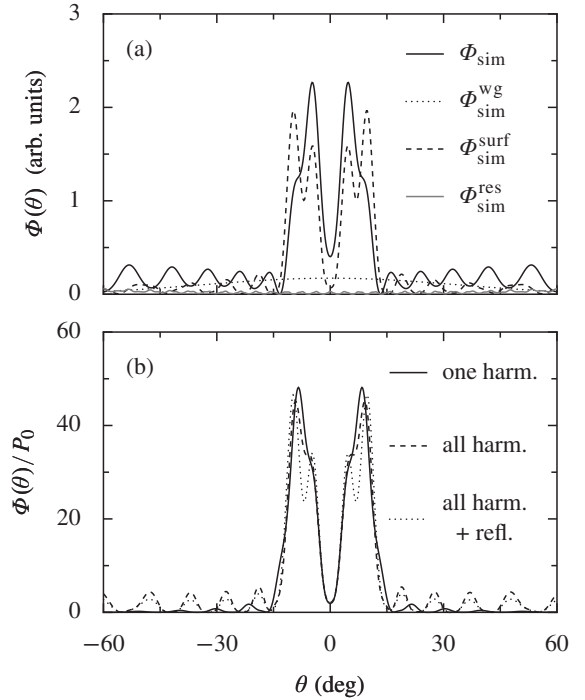


FIG. 7. (a) Angular dependence of the radiation intensity for crystal C with $N=9$ corrugations at frequency $\omega=0.400 \times 2\pi c/d$ calculated by the MS method. Solid black line: total radiation intensity; dotted line: contribution of the waveguide outlet region calculated by Eq. (2) with the integration interval restricted to $|x| < d/2$; dashed line: contribution of the surface region, with $d/2 < |x| < N\Lambda + d/2$; gray line: contribution of the crystal exterior, with $|x| > N\Lambda + d/2$. (b) Angular dependence of the radiation intensity for the same crystal and frequency value calculated on the basis of our model with the surface field expansion [Eq. (8)] truncated to a single harmonic (solid line) and to 17 harmonics (dashed and dotted lines). The data plotted with the dotted line result from computations taking into account surface wave reflections at the crystal boundaries.

main beams shift by several degrees toward the surface normal. As a result, they begin to overlap at frequency values below those predicted by leaky-wave considerations alone. This explains the discrepancy in position of the absolute maxima between the theoretical and the numerical curves in Fig. 6 mentioned in the previous subsection.

The radiation pattern in the large-angle ($\theta \geq 15^\circ$) region is also affected by the field stemming from the outlet: the destructive interference of this field with that emitted from the corrugated surface causes an offset of the sidelobe positions. The contribution of the residual radiation, however, remains negligible throughout the angular range covered by the plots in Fig. 7.

Let us compare the results presented in Fig. 7(a) with the predictions of our model plotted in Fig. 7(b). The solid curve has been calculated with the approximate leaky-mode structure factor [i.e., with the series in Eq. (8) truncated to a single term, as discussed in Sec. II]; the dashed line results from calculations with the full structure factor (with amplitudes of the individual harmonics computed numerically by the method outlined in Sec. III). In both curves, the main peaks



FIG. 8. Electric-field magnitude in the surface region of crystal B with $N=9$ corrugations at frequency $\omega=0.405 \times 2\pi c/d$. An interference pattern resulting from surface wave reflections at the crystal boundaries is clearly visible.

occur at $\theta_0 \approx 11^\circ$, in good agreement with the $\Phi_{\text{sim}}^{\text{surf}}$ curve plotted in Fig. 7(a). However, the field structure at angles far from θ_0 is seen to depend strongly on the structure factor; in general, the radiation intensity obtained with the one-harmonic approximation is much smaller than that calculated without this simplification. This may be the reason why at low-frequency values, the model-predicted $\Phi(\theta=0)$ value is very small compared to that resulting from MS calculations, since for these frequency values the surface normal lies far from the direction $\theta=\theta_0$.

Another difference between the theoretical plots in Fig. 7(b) and the $\Phi_{\text{sim}}^{\text{surf}}$ curve is a distinct dip of the latter at $\theta \approx 6^\circ$. This turns out to follow from surface wave reflections occurring at the crystal boundaries, which have been neglected in our model, but are of some importance for crystals with shallow corrugations (involving weakly leaky modes) or of small size; see Fig. 8. The dotted curve in Fig. 7(b) shows the radiation intensity angular dependence after taking these reflections into account, with the reflection coefficient at the surface termination calculated by the method outlined in Ref. 20. Evidently, this curve is in excellent agreement with the results of MS simulations.

Lastly, let us consider the frequency $\omega=0.420 \times 2\pi c/d$, which lies to the right of the main peak in the $\Phi_{\text{sim}}(\theta=0)$ curve shown in Fig. 6(b) and for which the model-predicted radiation intensity at $\theta=0$ is too large. Figure 9(a), a counterpart of Fig. 7(a), shows that at this frequency value, the radiation stemming from the waveguide output has magnitude larger than in the low-frequency case analyzed previously. However, since in the small-angle region it is out of phase with the field produced by the leaky modes, the total radiation intensity becomes significantly smaller than it would be without the direct beam from the waveguide outlet. In addition, as indicated in Fig. 9, neglecting higher harmonics in the surface field expansion used in the model-based calculations leads to some overestimation of the leaky-mode-induced radiation intensity at $\theta=0$. Together, these two factors explain the theory-versus-simulation discrepancy observed in Fig. 6 in the frequency range $\omega > 0.41 \times 2\pi c/d$.

V. DISCUSSION

As indicated in Fig. 6, maximum beam collimation occurs at a frequency value of around $0.41 \times 2\pi c/d$, which, according to Fig. 3, corresponds to surface modes with $k'_x \approx -0.01 \times 2\pi/d$ (crystal B) and $k'_x \approx -0.025 \times 2\pi/d$ (crystal C) rather than to modes from the center of the Brillouin zone ($k'_x=0$). Incidentally, the $k'_x=0$ modes, being delocalized (propagative inside the crystal), could not be responsible for beaming. However, the nonzero real part of the wave vector of the surface modes for which maximum beaming is ob-

served is easily explained on the basis of the model discussed in Sec. II. It is a consequence of the competition between the tendency to reduce $|k'_x|$ in order to obtain better phase matching of waves emitted from individual unit cells and, on the other hand, the negative effect of too large a k''_x on the effective length of the “grating.” Since in the negative- k'_x region a decrease in $|k'_x|$ is always accompanied by an increase in k''_x , the most intensive beaming occurs for moderate (“balanced”) values of both parameters.

The model also sheds light on why in negatively corrugated crystals, the frequency value corresponding to maximum beaming lies remarkably close to that of the surface mode from the edge of the unperturbed crystal surface Brillouin-zone ($k_x=\pi/d$). This proves to be a resultant of two opposing effects. It has been pointed out¹⁰ that bringing surface cylinders closer to the bulk crystal causes a blueshift of the surface-mode dispersion relation due to a decrease of the fraction of electromagnetic energy contained within the dielectric. However, since beaming occurs at nonzero k'_x values, this shift starts from an initial frequency value lower than that of the Brillouin-zone-edge mode (which moves to the new Brillouin zone center after an infinitesimal

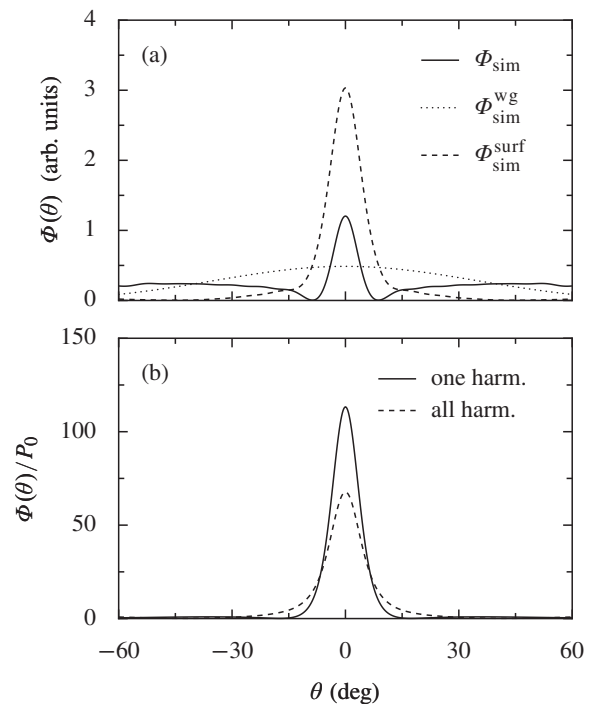


FIG. 9. Same as Fig. 7, but at frequency $\omega=0.420 \times 2\pi c/d$. Since at this frequency virtually no power reaches the crystal boundaries, $\Phi_{\text{sim}}^{\text{res}}(\theta)$ and the reflected surface wave contribution are not calculated.

$2d$ -periodic corrugation is introduced). As a consequence, the resultant optimum beaming frequency nears the original frequency of the $k_x = \pi/d$ mode.

The accuracy of the model could be considerably improved by taking into account the radiation emitted directly from the waveguide outlet. This, however, would require a detailed investigation of the interactions between the outlet and the surface cylinders in its immediate vicinity, as these interactions determine the amount of power transferred to surface modes and that emitted directly into free space. An analytical formulation of these effects seems hardly feasible, though.

VI. CONCLUSIONS

We have presented a quantitative analysis of a model explaining the effect of surface corrugation on the collimation of radiation leaving the outlet of a photonic crystal waveguide, on the basis of the dispersion relation of leaky modes supported by the corrugated surface. The dispersion relation has been calculated and discussed for a number of surface terminations. The model has been shown to reproduce the basic features of the investigated effect, and the significance of the factors left out of account has been evaluated. Besides clarifying the conditions necessary for optimum beaming, the model also explains the relative insensitivity of the maximum collimation frequency value to the degree of surface modulation. We believe that our results will contribute to a deeper understanding of the physical grounds of the beaming effect.

ACKNOWLEDGMENTS

I thank Henryk Puzkarski and Maciej Krawczyk for numerous useful discussions and encouragement during my work on this project.

APPENDIX: THE CHOICE OF BASIS STATES

In this section, we specify the selection rules for the states to be used as the expansion basis for fields in the homogeneous and periodically modulated system regions considered in Sec. III. Let us begin with the homogeneous region. Here, the electric field can be written as a Rayleigh expansion, i.e., a linear combination of spatial harmonics,

$$E(x, z) = \sum_n A_n e^{i(k_{xn}x + k_{zn}z)}, \quad (\text{A1})$$

where $k_{xn} = k_x + 2\pi n/\Lambda$, and the condition $k_{zn}^2 = k_0^2 - k_{xn}^2$ holds; k_x and k_0 are fixed. For real k_x , the obvious choice for the sign of k_{zn} is

$$k_{zn} > 0 \quad \text{if } k_{zn}^2 > 0, \quad (\text{A2a})$$

$$k_{zn}/i > 0 \quad \text{if } k_{zn}^2 < 0, \quad (\text{A2b})$$

so that the propagating harmonics [Eq. (A2a)] carry energy in the $+z$ direction, and the evanescent ones [Eq. (A2b)] decay with $z \rightarrow \infty$. When k_x is complex, the sign of k_{zn} should be chosen so as to assure analytical continuity with the $k_x \in \mathbb{R}$ case, i.e.,

$$\text{Re } k_{zn} > 0 \quad \text{if } \text{Re } k_{zn}^2 > 0, \quad (\text{A3a})$$

$$\text{Im } k_{zn} > 0 \quad \text{if } \text{Re } k_{zn}^2 < 0. \quad (\text{A3b})$$

It is easy to show that these rules can be combined into

$$\text{Re } k_{zn} + \text{Im } k_{zn} > 0, \quad (\text{A4})$$

in accordance with Refs. 16 and 21.

In the semi-infinite PC, the field can be expanded in the crystal eigenstates corresponding to the fixed k_x and k_0 . For real k_x , these eigenstates are either purely propagative in the z direction, with $k_z \in \mathbb{R}$, or purely evanescent, with $k_z = ik_z''$ or $k_z = \pm \pi/d + ik_z''$, where $k_z'' \in \mathbb{R}$. In the former case, the states to be included in the expansion are those with negative z component of their energy flux vector \mathcal{E} , and in the latter case, those decaying when z approaches $-\infty$, i.e., those with $k_z'' < 0$. When k_x is allowed to be complex, the k_z component of a crystal eigenstate wave vector can take arbitrary complex values too. However, the eigenmodes can still be classified as “essentially propagative,” with $k_z = k_z' + ik_z''$ fulfilling the condition

$$|k_z''| < |k_z'| \quad \text{and} \quad |k_z''| < \pi/d - |k_z'|, \quad (\text{A5})$$

and “essentially evanescent” otherwise. States of these two families to be included in the expansion should then be selected according to the $\mathcal{E} \cdot \hat{z} < 0$ and $k_z'' < 0$ rules, respectively.

*Electronic address: achu@hoth.amu.edu.pl

¹A. Mekis and J. D. Joannopoulos, *J. Lightwave Technol.* **19**, 861 (2001).

²A. Håkansson, P. Sanchis, J. Sánchez-Dehesa, and J. Martí, *J. Lightwave Technol.* **23**, 3881 (2005).

³E. Moreno, F. J. García-Vidal, and L. Martín-Moreno, *Phys. Rev. B* **69**, 121402(R) (2004).

⁴P. Kramper, M. Agio, C. M. Soukoulis, A. Birner, F. Müller, R. B. Wehrspohn, U. Gösele, and V. Sandoghdar, *Phys. Rev. Lett.* **92**, 113903 (2004).

⁵H. J. Lezec, A. Degiron, E. Devaux, R. A. Linke, L. Martín-Moreno, F. J. García-Vidal, and T. W. Ebbesen, *Science* **297**, 820 (2002).

⁶E. Moreno, L. Martín-Moreno, and F. J. García-Vidal, *Photonics Nanostruct. Fundam. Appl.* **2**, 97 (2004).

⁷W. R. Frei, D. A. Tortorelli, and H. T. Johnson, *Appl. Phys. Lett.* **86**, 111114 (2005).

⁸S. K. Morrison and Y. S. Kivshar, *Appl. Phys. Lett.* **86**, 111110 (2005).

⁹S. K. Morrison and Y. S. Kivshar, *Appl. Phys. B: Lasers Opt.* **81**,

- 343 (2005).
- ¹⁰S. K. Morrison and Y. S. Kivshar, Proc. SPIE **5733**, 104 (2005).
- ¹¹I. Bulu, H. Caglayan, and E. Ozbay, Opt. Lett. **30**, 3078 (2005).
- ¹²E. V. Jull, *Aperture Antennas and Diffraction Theory* (Peter Peregrinus, New York, 1981), p. 13.
- ¹³F. K. Schwering and S. T. Peng, IEEE Trans. Microwave Theory Tech. **31**, 199 (1983).
- ¹⁴E. Istrate, A. A. Green, and E. H. Sargent, Phys. Rev. B **71**, 195122 (2005).
- ¹⁵E. Popov and B. Bozhkov, Appl. Opt. **39**, 4926 (2000).
- ¹⁶S. T. Peng, T. Tamir, and H. L. Bertoni, IEEE Trans. Microwave Theory Tech. **23**, 123 (1975); **24**, 542 (1976).
- ¹⁷Y. Ding and R. Magnusson, Opt. Express **15**, 680 (2007).
- ¹⁸L. O. Goldstone and A. A. Oliner, IRE Trans. Antennas Propag. **7**, 307 (1959).
- ¹⁹D. Felbacq, G. Tayeb, and D. Maystre, J. Opt. Soc. Am. A **11**, 2526 (1994).
- ²⁰W. Śmigaj, arXiv:physics/0703165 (unpublished).
- ²¹M. Neviere, in *Electromagnetic Theory of Gratings*, edited by R. Petit (Springer, Berlin, 1980), pp. 123–158.